DIGITAL ACCESS TO SCHOLARSHIP AT HARVARD
DASH.HARVARD.EDU

HARVARD LIBRARY

Synthesis and patterning of tunable multiscale materials with engineered cells

Citation

Chen, Allen Y., Zhengtao Deng, Amanda N. Billings, Urartu O.S. Seker, Michelle Y. Lu, Robert J. Citorik, Bijan Zakeri, and Timothy K. Lu. 2014. "Synthesis and patterning of tunable multiscale materials with engineered cells." Nature materials 13 (5): 515-523. doi:10.1038/nmat3912. http://dx.doi.org/10.1038/nmat3912.

Published version

https://doi.org/10.1038/nmat3912

Link

http://nrs.harvard.edu/urn-3:HUL.InstRepos:13454699

Terms of use

This article was downloaded from Harvard University's DASH repository, and is made available under the terms and conditions applicable to Other Posted Material (LAA), as set forth at
https://harvardwiki.atlassian.net/wiki/external/NGY5NDE4ZjgzNTc5NDQzMGIzZWZhMGFlOWI2M2EwYTg

Accessibility

https://accessibility.huit.harvard.edu/digital-accessibility-policy

Share Your Story

The Harvard community has made this article openly available.
Please share how this access benefits you. Submit a story

NIH Public Access
Author Manuscript
Nat Mater. Author manuscript; available in PMC 2014 November 01.

Published in final edited form as:
Nat Mater. 2014 May ; 13(5): 515–523. doi:10.1038/nmat3912.

Synthesis and patterning of tunable multiscale materials with engineered cells

Allen Y. Chen[1,2,3,4,6], **Zhengtao Deng**[2,3,4], **Amanda N. Billings**[3], **Urartu O.S. Seker**[2,3,4], **Michelle Y. Lu**[2,3,4], **Robert J. Citorik**[2,3,4,5], **Bijan Zakeri**[2,3,4], and **Timothy K. Lu**[1,2,3,4,5,*]

[1]Biophysics Program, Harvard University, Cambridge, MA 02138, USA

[2]Department of Electrical Engineering & Computer Science, Massachusetts Institute of Technology, 77 Massachusetts Avenue, Cambridge, MA 02139, USA

[3]Department of Biological Engineering, Massachusetts Institute of Technology, 77 Massachusetts Avenue, Cambridge, MA 02139, USA

[4]MIT Synthetic Biology Center, 500 Technology Square, Cambridge MA 02139, USA

[5]MIT Microbiology Program, 77 Massachusetts Avenue, Cambridge MA 02139, USA

[6]Harvard-MIT Health Sciences and Technology, Institute for Medical Engineering and Science, 77 Massachusetts Avenue, Cambridge, MA 02139, USA.

Abstract

Many natural biological systems - such as biofilms, shells and skeletal tissues - are able to assemble multifunctional and environmentally responsive multiscale assemblies of living and non-living components. Here, by using inducible genetic circuits and cellular communication circuits to regulate *Escherichia coli* curli amyloid production, we show that *E. coli* cells can organize self-assembling amyloid fibrils across multiple length scales, producing amyloid-based materials that are either externally controllable or undergo autonomous patterning. We also interfaced curli fibrils with inorganic materials, such as gold nanoparticles (AuNPs) and quantum dots (QDs), and used these capabilities to create an environmentally responsive biofilm-based electrical switch, produce gold nanowires and nanorods, co-localize AuNPs with CdTe/CdS QDs to modulate QD fluorescence lifetimes, and nucleate the formation of fluorescent ZnS QDs. This work lays a foundation for synthesizing, patterning, and controlling functional composite materials with engineered cells.

Natural multicellular assemblies such as biofilms, shells, and skeletal tissues have distinctive characteristics that would be useful for materials production and patterning[1-9]. They can detect external signals and respond via remodelling, implement patterning across different

*Correspondence to: T.K.L (timlu@mit.edu)..

Author contributions T.K.L. and A.Y.C. conceived the experiments. A.Y.C., Z.D., A.N.B., U.O.S., M.Y.L., and R.J.C. performed the experiments, A.Y.C., Z.D., A.N.B., and T.K.L. analysed the data, discussed results, and wrote the manuscript.

Additional information Supplementary information is available in the online version of the paper. Reprints and permissions information is available online at www.nature.com/reprints. Correspondence and requests for materials should be addressed to T.K.L.

Competing financial interests The authors declare competing financial interests. T.K.L. and A.Y.C. have filed a provisional application with the US Patent and Trademark Office on this work.

NIH-PA Author Manuscript
NIH-PA Author Manuscript
NIH-PA Author Manuscript

NIH-PA Author Manuscript

NIH-PA Author Manuscript

NIH-PA Author Manuscript

length scales, and organize inorganic compounds to create organic-inorganic composites. In this work, such systems provide inspiration for the design of environmentally responsive systems that can integrate biotic and abiotic materials via hierarchical self-assembly. To achieve these capabilities, we engineered artificial gene circuits and self-assembling amyloid fibrils together with synthetic cellular consortia[10-16] and abiotic materials.

Our model system is curli, an extracellular amyloid material produced by *E. coli* that forms fibrils based on the self-assembly of the secreted major curli subunit CsgA[17]. Secreted CsgA monomers are templated on CsgB, which is anchored to the cell surface, to form curli fibrils; moreover, CsgA secreted from one cell can interact with CsgB on other cells[17]. Using synthetic riboregulators[18], we implemented inducible transcriptional and translational control over the expression of CsgA subunits engineered to display various peptide tags, which can interface with inorganic materials. We transformed our synthetic circuits into an *E. coli* MG1655 *PRO* Δ*csgA ompR234* host strain (see Supplementary Table 3 and Supplementary Fig. 20), which has the endogenous *csgA* gene deleted. The *ompR234* mutation enables curli production in liquid media at 30°C by enhancing the expression of genes from the native curli operon, including *csgB*[19,20]. We first introduced histidine-tagged CsgA ($CsgA_{His}$) expression under tight regulation by an anhydrotetracycline (aTc) inducer-responsive riboregulator[18] (Fig. 1a). $CsgA_{His}$ contained two histidine tags, one inserted before the first repeat domain and one inserted after the last repeat domain in CsgA (Supplementary Table 1). The resulting cell strain was designated $aTc_{Receiver}/CsgA_{His}$. Immuno-gold labelling experiments with anti-CsgA antibodies (M. Chapman, University of Michigan[21,22]) showed that curli fibrils were only produced in the presence of aTc (Fig. 1b and Supplementary Fig. 1). Using confocal microscopy, we characterized biofilms formed by $aTc_{Receiver}/CsgA_{His}$ cells augmented with an mCherry-expressing plasmid for convenient visualization. This strain formed biofilms only when induced by aTc, both under static culture conditions (Fig. 1c and Supplementary Fig. 2a) and when cultured in microfluidic flow cells (Fig. 1d and Supplementary Fig. 2b). Biofilm growth was confirmed with a standard crystal-violet (CV) assay (Supplementary Fig. 3). We also quantified curli production with dot blots and found a yield of 63±5.8 (s.e.m.) mg/cm^3 of biofilm after 24h (Supplementary Fig. 22).

To create engineered cellular consortia for materials patterning, we built three additional strains: one with CsgA under regulation by an acyl-homoserine lactone (AHL)-inducible riboregulator ($AHL_{Receiver}/CsgA$), one with CsgA under regulation by an aTc-inducible riboregulator ($aTc_{Receiver}/CsgA$), and one with $CsgA_{His}$ under regulation by an AHL-inducible riboregulator ($AHL_{Receiver}/CsgA_{His}$). These strains only produced curli fibrils in the presence of the cognate inducer, demonstrating tight and orthogonal regulation of *csgA* and $csgA_{His}$ expression (Supplementary Fig. 8). Moreover, insertion of heterologous histidine tags did not interfere with curli fibril formation based on Congo Red assays and TEM imaging (Supplementary Fig. 4 and 5).

Externally controllable patterning

We engineered consortia composed of $AHL_{Receiver}/CsgA$ and $aTc_{Receiver}/CsgA_{His}$ cells to produce two-component protein fibrils composed of CsgA and $CsgA_{His}$ (Fig. 2). By tuning

NIH-PA Author Manuscript

NIH-PA Author Manuscript

NIH-PA Author Manuscript

the pulse lengths and pulse amplitudes of AHL and/or aTc, fibrils with different structures and compositions were formed. For example, we mixed equal numbers of $AHL_{Receiver}$/CsgA and $aTc_{Receiver}$/$CsgA_{His}$ cells together and induced this mixed-cell population first with AHL, followed by aTc (Fig. 2a). In analogy to block co-polymers, this produced block "co-fibrils" consisting of blocks of CsgA (unlabelled fibril segments) and blocks of $CsgA_{His}$ (fibril segments labelled by nickel nitrilotriacetic acid-conjugated gold particles (NiNTA-AuNPs). NiNTAAuNPs specifically labelled $CsgA_{His}$-based curli fibrils but not CsgA-based curli fibrils (Supplementary Fig. 9).

We tuned the length distribution of the CsgA and $CsgA_{His}$ blocks, as well as the relative proportions of CsgA and $CsgA_{His}$, by changing the relative lengths of AHL pulses versus aTc pulses. As AHL induction time increased, non-NiNTA-AuNP-labelled fibril segments increased in length, indicating longer CsgA blocks (Fig. 2b and Supplementary Fig. 6a). At the same time, the proportion of fibril length labelled with NiNTA-AuNP decreased, indicating a higher relative proportion of CsgA in the fibrils (Fig. 2b). With temporal separation in expression, the distinct CsgA and $CsgA_{His}$ segments within the block co-fibrils were longer than those in co-fibrils assembled when CsgA and $CsgA_{His}$ were secreted simultaneously with no temporal separation, even though the overall CsgA to $CsgA_{His}$ ratios were similar (Supplementary Fig. 6a). Thus, engineered cells can translate the temporal interval length of input signals into different nanoscale structures and compositions of materials.

We also tuned the length distributions of the two types of blocks, as well as their relative proportions, by inducing simultaneous expression of the CsgA variants with different concentrations of AHL and aTc (Fig. 2c). With AHL-only induction, fibrils were almost uniformly unlabelled; with increasing aTc concentration, the population as well as lengths of unlabelled fibril segments decreased while those of labelled fibril segments increased (Fig. 2d, Supplementary Fig. 6b). With aTc-only induction, fibrils were almost uniformly labelled by NiNTA-AuNPs; with increasing AHL concentration, the population as well as lengths of unlabelled segments increased (Supplementary Fig. 7). Thus, engineered cells can translate the amplitudes of input signals, such as inducer concentrations, into different nanoscale structures and compositions of materials.

Autonomous patterning

Cellular communities containing synthetic cellular communication circuits[23-26] can autonomously produce dynamic materials whose structure and composition changes with time (Fig. 3). Since *E. coli* does not normally produce AHL, we first engineered an *E. coli* strain that constitutively produces AHL and inducibly produces CsgA in the presence of aTc (AHL_{Sender}+$aTc_{Receiver}$/CsgA). This strain communicated with $AHL_{Receiver}$/$CsgA_{His}$ cells via the diffusible cellular communication signal, AHL. We then combined AHL_{Sender}+$aTc_{Receiver}$/CsgA and $AHL_{Receiver}$/$CsgA_{His}$ cells in varying ratios (Fig. 3a). Induction of this mixed-cell population by aTc resulted in CsgA secretion. Over time, AHL accumulation led to increasing secretion of $CsgA_{His}$, thus generating an increased population and lengths of $CsgA_{His}$ blocks, and a higher relative proportion of $CsgA_{His}$ in material composition (Fig. 3b and Supplementary Fig. 10). The temporal dynamics of

NIH-PA Author Manuscript

NIH-PA Author Manuscript

NIH-PA Author Manuscript

changes in material composition was tunable by the initial seeding ratio of AHL_{Sender}+$aTc_{Receiver}$/CsgA to $AHL_{Receiver}$/$CsgA_{His}$ cells (Fig. 3b). When only AHL_{Sender}+$aTc_{Receiver}$/CsgA cells were present, fibrils were almost uniformly unlabelled; when only $AHL_{Receiver}$/$CsgA_{His}$ cells were present, no fibrils were formed (Fig. 3b).

Multiscale patterning

In addition, engineered cellular consortia can achieve spatial control over multiple length scales. Genetic regulation of subunit expression allows fibril patterning from tens of nanometres to micrometres, while spatial control at the macroscale can be achieved via spatially varying inducer concentrations. These two methods of control can be combined to create materials patterned across multiple length scales (Fig. 4). To demonstrate this, we created agar plates with opposing concentration gradients of AHL and aTc and overlaid bacterial populations consisting of equal numbers of four cell strains: $AHL_{Receiver}$/CsgA, $aTc_{Receiver}$/$CsgA_{His}$, $AHL_{Receiver}$/GFP, and $aTc_{Receiver}$/mCherry. The $AHL_{Receiver}$/GFP and $aTc_{Receiver}$/mCherry cells enabled visualization of inducer concentration gradients (Fig. 4b and Supplementary Fig. 12). $AHL_{Receiver}$/CsgA and $aTc_{Reciever}$/$CsgA_{His}$ cells secreted different levels of CsgA and $CsgA_{His}$, depending on their positions on the concentration gradient, to generate a spatial gradient of changing fibril structures (Fig. 4a). This multiscale material was patterned at the nanoscale as block co-fibrils and at the millimetre scale with position-dependent fibril structure (Fig. 4b and Supplementary Fig. 11a). Agar plates without inducer concentration gradients did not generate fibril structures that varied along the plate (Supplementary Fig. 11a).

Protein engineering can also control the structure of cell-produced biomaterials at the nanoscale. We hypothesized that fusing tandem repeats of CsgA together would increase the distance between equivalent positions on adjacent monomers where functional domains can be displayed. Concatenating eight tandem repeats of CsgA and adding a histidine tag to the C-terminus ($8XCsgA_{His}$) resulted in fibrils that were labelled by a syncopated pattern of NiNTA-AuNP, with clusters of particles separated by 33.3±27.1 (s.e.m.) nm (Fig. 4c and Supplementary Fig. 11b). Using this finding, we demonstrated a second example of multiscale assembly. Specifically, we combined equal numbers of $AHL_{Receiver}$/$8XCsgA_{His}$ and $aTc_{Receiver}$/$CsgA_{His}$ cells. We induced this mixed-cell population sequentially with AHL followed by aTc (Fig. 4d) to generate block co-fibrils consisting of $8XCsgA_{His}$ segments and $CsgA_{His}$ segments patterned across the nanometre to micrometre scales (Fig. 4d and Supplementary Fig. 11c).

Interfaces with inorganic materials

Our living cell system can be used to create functional materials, such as environmentally switchable conductive biofilms. We hypothesized that aTc-inducible production of $CsgA_{His}$ monomers by $aTc_{Receiver}$/$CsgA_{His}$ cells would generate extracellular amyloid fibrils that organize NiNTA-AuNPs into chains and form a conductive biofilm network. As shown in Figure 1, the expression of extracellular curli fibrils enables surface adherence by multicellular bacterial communities, resulting in biofilm formation. Engineered biofilms were grown on interdigitated electrodes deposited on Thermanox coverslips, with

NIH-PA Author Manuscript

NIH-PA Author Manuscript

NIH-PA Author Manuscript

$aTc_{Receiver}/CsgA_{His}$ cells cultured in the presence of NiNTA-AuNPs and in the presence or absence of aTc inducer (Fig. 5a). We showed by confocal microscopy that biofilms were formed in an aTc-dependent manner (Supplementary Fig. 14). Scanning electron microscopy (SEM), scanning electron microscopy/energy dispersive X-ray spectroscopy (SEM/EDS), and transmission electron microscopy (TEM) were performed to further characterize biofilm samples (Fig. 5b). In the presence of aTc, biofilms formed, spanned electrodes (as shown by SEM imaging), and contained networks of gold that connected electrodes (as shown by SEM/EDS elemental mapping). In contrast, SEM imaging of cells grown in the absence of induction showed only scattered bacteria in the gaps between electrodes, and SEM/EDS showed no gold networks. TEM imaging revealed that aTc-induced biofilms organized gold particles into dense networks (Fig. 5b and Supplementary Fig. 16), while samples with cells in the absence of aTc showed only scattered, isolated gold particles (Fig. 5b). Biofilms formed in the presence of aTc had 0.82±0.17 (s.e.m.) nanosiemens conductance, whereas samples with cells in the absence of aTc had no measureable conductance (Supplementary Fig. 15). Biofilms formed with $aTc_{Receiver}/CsgA_{His}$ cells induced by aTc, but grown in the absence of NiNTA-AuNPs, had electrical conductance that was two orders of magnitude lower than those formed in presence of NiNTA-AuNPs (Supplementary Fig. 17a). Samples containing $AHL_{Receiver}/CsgA_{His}$ cells grown in the presence of NiNTA-AuNPs and aTc had no measureable conductance (Supplementary Fig. 17b).

We extended cell-based gold-particle patterning to create nanowires and nanorods via additional gold deposition. When $aTc_{Receiver}/CsgA_{His}$ and $AHL_{Receiver}/CsgA$ cells were induced with only aTc, the resulting curli fibrils templated gold nanowires. When the cells were induced with both aTc and AHL, the resulting co-fibrils contained $CsgA_{His}$ and CsgA which templated consecutive gold nanorods (Fig. 5c). Gold nanorods have been studied for a range of applications because of their more broadly tunable absorption spectra compared to nanoparticles, which allows for peak absorption in the near-IR window used for *in vivo* imaging and photothermal ablation[27]. Moreover, via conjugation with targeting ligands and drug molecules, they can also act as targeted drug delivery vehicles for therapeutic and diagnostic applications[28,29].

We also used cellular biofabrication to create co-fibrils that assembled CdTe/CdS quantum dots (QDs) with gold nanoparticles, resulting in the modulation of QD fluorescence (Fig. 6). We leveraged interactions between the SpyCatcher protein and the SpyTag peptide tag[30], which results in the formation of covalent bonds, to dock QDs to fibrils displaying SpyTag. We used an orthogonal interaction between anti-FLAG antibodies and the FLAG affinity tag to dock 40nm gold particles to fibrils displaying the FLAG tag. $CsgA_{SpyTag}$ fibrils were specifically bound by SpyCatcher-conjugated CdTe/CdS QDs (QD-SpyCatcher, Supplementary Fig. 21), while $CsgA_{FLAG}$ fibrils were specifically bound by anti-FLAG antibodies which were in turn bound by 40nm gold particles conjugated with secondary antibodies (Fig. 6a, Supplementary Fig. 23a, b). $AHL_{Receiver}/CsgA_{SpyTag}$ and $aTc_{Receiver}/CsgA_{FLAG}$ strains were co-cultured in the presence of AHL, aTc, or both AHL and aTc. In the presence of AHL, fibrils produced by the cellular consortia only bound QD-SpyCatcher, whereas in the presence of aTc, the resulting fibrils only bound antibody-conjugated 40nm

NIH-PA Author Manuscript

NIH-PA Author Manuscript

NIH-PA Author Manuscript

gold particles (Fig. 6b and Supplementary Fig. 18). When both inducers were present, the fibrils co-assembled QDs with gold nanoparticles (Fig. 6b). Characterization with fluorescence-lifetime imaging microscopy (FLIM) revealed that co-assemblies of QDs and gold nanoparticles had altered fluorescence lifetimes and intensities compared to assemblies of QDs alone (Fig. 6c).

These results demonstrate that the behaviour of stimuli-responsive materials can be modulated by curli fibrils patterned with engineered cells. AuNP-QD heterostructures are of interest because plasmon-exciton interactions between plasmonic AuNPs and fluorescent QDs allow for tailoring of photon emission properties. By selecting appropriate materials and architectures, one can potentially tune emission intensity, directionality, and spectral profile for a range of applications[31-34].

In addition to organizing pre-formed nanomaterials, cell-fabricated curli fibrils can be used to grow inorganic materials. To demonstrate this, we engineered a strain that produced curli fibrils displaying a ZnS-nucleating peptide ($CsgA_{ZnS\ peptide}$, Supplementary Table 1)[35]. The resulting fibrils nucleated ~5nm particles (Fig. 6d), whereas control fibrils composed of wild-type CsgA nucleated few such particles (Supplementary Fig. 23c). HRTEM images revealed that the nucleated particles had a cubic zinc blende ZnS (111) structure with a typical crystalline spacing of 0.31nm (Fig. 6d). EDS analysis of elemental composition showed an approximately 1:1 ratio of zinc and sulphur (Fig. 6d). These data indicate that the particles are ZnS nanocrystals. The nanocrystals were fluorescent, with an emission peak at 490nm when excited at 405nm (Fig. 6d).

Outlook

We have shown that protein-based amyloid fibrils produced by living cells can be interfaced with different inorganic materials via a range of strategies. Beyond being a convenient model system with which to explore the applications of living systems to materials science, protein materials are of practical interest because they constitute a major class of biomaterials[36]. Protein materials can have programmable structures[37] and diverse functionalities, such as responsiveness to physicochemical stimuli[38], the ability to interact with living systems[39], and the ability to organize abiotic materials for expanded functionalities[35,40-42]. Amyloid fibrils can provide beneficial materials properties such as resistance to degradation and mechanical strength comparable to that of steel[43]. As we have shown here, amyloid fibrils assembled by cells constitute a versatile scaffold that can co-organize and synthesize fluorescent QDs as well as gold nanowires, nanorods, and nanoparticles. This approach could be generalized to include multiple CsgA variants with different functional properties and abilities to interact with various inorganic materials. In addition, curli fibrils with tunable structure and composition could be used as patterned scaffolds for multi-enzyme systems by displaying orthogonal affinity tags on curli fibrils which interact with different enzymes.

Most existing examples of protein biomaterials are assembled *in vitro* from chemically synthesized peptides or purified subunits and do not take full advantage of the fact that the materials' constituent subunits can be integrated into living cell communities. Living cells

NIH-PA Author Manuscript

NIH-PA Author Manuscript

NIH-PA Author Manuscript

are natural platforms for engineering multiscale patterned materials because biology is organized in a hierarchical manner, from macromolecules (e.g. proteins, nucleic acids, carbohydrates, lipids) to macromolecular assemblies (synthetic variants of which are used as nanomaterials[37,44-46]) to organelles to cells and to tissues. In fact, natural biological materials such as bone are hierarchically organized to fulfil varied functional requirements[1,9]. Thus, we have demonstrated an engineered cellular platform that synthesizes and patterns self-assembling materials with controllable functionality, structure, and composition.

Using gene circuits within engineered biofilms for multiscale patterning of materials is a novel application area for synthetic biology. This work applies useful characteristics of multicellular communities to materials fabrication and builds upon previous efforts to engineer biofilms with synthetic circuits[10-16]. This strategy can be expanded to other cellular and biomaterials contexts for applications ranging from biointegrated electronic and optical devices[47-49] to tissue engineering scaffolds[50]. For example, cells designed to compute and integrate complex signals could be used to assemble functional materials in response to their environment[18,19]. These “smart” living materials could be composed of specialized cellular consortia that coordinate with each other for multi-functional materials synthesis. Mammalian cells capable of tunable, environmentally responsive synthesis of multiscale materials could be used to mimic the dynamic microenvironment of *in vivo* extracellular matrices[51] for tissue engineering. Our demonstration of a gradient material patterned at the nanoscale and the millimetre scale could be used to biofabricate functionally graded materials[52]. Moreover, leveraging hierarchical organization from biology for multiscale patterning should complement other strategies for materials synthesis that require directed intervention[53], such as 3D printing[52]. Repeated materials-synthesis processes or environmentally switchable behaviours could be achieved by triggering biofilm disassembly[12,13,54].

In summary, by integrating synthetic gene networks in engineered cells with extracellular protein biomaterials, living materials with environmental responsiveness, tunable functionalities, multiscale patterning, and even the ability to self-heal and remodel could be realized. In such materials, there would be a division of labour between cells (providing functionalities of living systems)[55], extracellular protein materials (providing spatial patterning and structural integrity), and interfaced abiotic materials (providing functionalities of non-living systems). Thus, we envision that engineering artificial cellular consortia, such as biofilms, to synthesize and organize heterogeneous functional materials will enable the realization of smart composite materials that combine the properties of living and non-living systems.

Methods Summary

Culture conditions

Seed cultures were inoculated from glycerol stocks and grown in LB-Miller medium for 12h at 37°C. Experimental cultures were grown at 30°C in M63 minimal medium supplemented with 1mM $MgSO_4$ and with 0.2% w/v glucose or 0.2% w/v glycerol. For inducing

NIH-PA Author Manuscript

NIH-PA Author Manuscript

NIH-PA Author Manuscript

conditions, anhydrotetracycline (Sigma) at concentrations of 1-250ng/ml and N-(β-ketocaproyl)-L-homoserine lactone (Sigma) at concentrations of 1-1000nM were used.

Anti-CsgA immuno-labelling

Rabbit anti-CsgA primary antibody (M. Chapman, University of Michigan) was used at 1:1000 dilution, goat anti-rabbit secondary antibody conjugated to 10nm gold particles (Sigma) was used at 1:10 dilution.

NiNTA-AuNP labelling

For specific binding of NiNTA-AuNP (Nanoprobes) to histidine tags displayed on curli fibrils, buffer consisting of 1X PBS with 0.487M NaCl, 80mM imidazole, and 0.2v/v% Tween20 was used.

Conductive biofilm conductance measurement

Interdigitated electrodes (IDEs) for measuring biofilm conductance were created by sputtering gold through custom shadowing masks (Tech-Etch) onto Thermanox coverslips (Nunc). IDEs were placed in 24-well plate wells and conductive biofilms grown by adding 100nM NiNTA-AuNP into culture medium. After biofilm culture, IDEs were washed by repeatedly immersing in ddH_2O, laid on a flat surface, and allowed to air dry for three days. A Keithley 4200 picoammeter with two-point probe was used to carry out a voltage sweep.

Gold nanowire and nanorod synthesis

Gold was specifically deposited on NiNTA-AuNP chains using GoldEnhance™ EM kit (Nanoprobes).

Specific binding of QD-SpyCatcher

For specific binding of CdTe/CdS-SpyCatcher to SpyTag peptide tags displayed on curli fibrils, buffer consisting of 1X PBS + 350mM NaCl + 0.3v/v% Tween20 was used.

Specific binding of antibody-conjugated 40nm AuNP

Rabbit anti-FLAG primary antibody (Sigma) was used at 1:250 dilution, goat anti-rabbit secondary antibody conjugated to 40nm AuNPs (Abcam) was used at 1:10 dilution.

Zinc sulphide nanocrystal synthesis

Fibril samples were incubated with 1μM $ZnCl_2$ at RT for 12h, followed by addition of 1μM Na_2S. Samples were then incubated at 0°C for 24h by packing in ice and placing in a 4°C room, and subsequently allowed to age for 12h at RT.

Transmission electron microscopy

Samples were deposited on 200-mesh formvar/carbon coated nickel TEM grids and stained with 2% uranyl acetate. TEM images were obtained on a FEI Tecnai Spirit transmission electron microscope operated at 80kV accelerating voltage. High-resolution transmission electron microscopy (HRTEM) and energy-dispersive X-ray spectroscopy (EDS) were performed on a JEOL 2010F electron microscope operating at 200 kV.

NIH-PA Author Manuscript

NIH-PA Author Manuscript

NIH-PA Author Manuscript

Scanning electron microscopy

Samples were imaged with a JEOL JSM-6010LA scanning electron microscope operated at 10kV accelerating voltage. Images were obtained in secondary electron imaging (SEI) mode, and elemental mapping was performed with energy-dispersive X-ray spectroscopy (EDS).

Fluorescence microscopy

Fluorescence-lifetime imaging microscopy (FLIM) was performed with a Zeiss 710 NLO multiphoton microscope with 20X objective and connected to a time-correlated single-photon counting system (Becker & Hickl). The excitation source was a 2-photon laser (Coherent Chameleon Vision II) tuned to 800nm, and emission was detected through a 590-650nm bandpass filter. Lambda scan analysis of fluorescent ZnS nanocrystals was performed with a Zeiss LSM 710 NLO Laser Scanning Confocal with 10X objective and 405nm excitation laser.

Supplementary Material

Refer to Web version on PubMed Central for supplementary material.

Acknowledgments

We thank J.J. Collins (Biomedical Engineering, Boston University) for donating riboregulator plasmids, R. Weiss (Electrical Engineering and Computer Science, MIT) for the gift of a LuxI plasmid, C. Dorel (Biosciences Department, INSA Lyon) for the gift of *E. coli* MG1655 *ompR234*, M. Chapman (Department of Molecular, Cellular, and Developmental Biology, University of Michigan Ann Arbor) for the gift of anti-CsgA antibodies, K. Ribbeck (Department of Biological Engineering, MIT) for use of confocal microscopy facilities, and L. Cameron (Confocal and Light Microscopy Core, Dana Farber Cancer Institute) for assistance with FLIM. We thank C. Zhong, K. Lowenhaupt, and P. Siuti from the Lu lab, S. Keating from the lab of Neri Oxman (Media Lab, MIT), K. Frederick from the lab of Susan Lindquist, Susan Lindquist (Whitehead Institute), and E. Dreaden from the lab of Paula Hammond (Chemical Engineering, MIT) for helpful discussions. We thank C. Zhong from the Lu lab for the gift of purified CsgA protein. We also thank M. Mimee and O. Purcell from the Lu lab for a close reading of this manuscript. This work was supported by the Office of Naval Research and the Army Research Office. This work was also supported in part by the MRSEC Program of the National Science Foundation under award number DMR-0819762. A.Y.C. acknowledges graduate research support from the Hertz Foundation, the Department of Defense, and NIH Medical Scientist Training Program grant T32GM007753. A.N.B. acknowledges support from NIH-NIEHS Training Grant in Toxicology 5 T32 ES7020-37. T.K.L. acknowledges support from the Presidential Early Career Award for Scientists and Engineers and the NIH New Innovator Award (1DP2OD008435).

References

1. Fratzl P, Weinkamer R. Nature's hierarchical materials. Progress in Materials Science. 2007; 52:1263–1334. doi:http://dx.doi.org/10.1016/j.pmatsci.2007.06.001.
2. Kollmannsberger P, Bidan CM, Dunlop JWC, Fratzl P. The physics of tissue patterning and extracellular matrix organisation: how cells join forces. Soft Matter. 2011; 7:9549–9560. doi: 10.1039/c1sm05588g.
3. Stevens MM, George JH. Exploring and engineering the cell surface interface. Science. 2005; 310:1135–1138. doi:10.1126/science.1106587. [PubMed: 16293749]
4. O'Toole G, Kaplan HB, Kolter R. Biofilm formation as microbial development. Annu Rev Microbiol. 2000; 54:49–79. doi:10.1146/annurev.micro.54.1.4954/1/49 [pii]. [PubMed: 11018124]
5. Epstein AK, Pokroy B, Seminara A, Aizenberg J. Bacterial biofilm shows persistent resistance to liquid wetting and gas penetration. Proc Natl Acad Sci U S A. 2011; 108:995–1000. doi: 1011033108 [pii]10.1073/pnas.1011033108. [PubMed: 21191101]

NIH-PA Author Manuscript NIH-PA Author Manuscript NIH-PA Author Manuscript

6. Belcher AM, et al. Control of crystal phase switching and orientation by soluble mollusc-shell proteins. Nature. 1996; 381:56–58.
7. Su XW, Zhang DM, Heuer AH. Tissue Regeneration in the Shell of the Giant Queen Conch, Strombus gigas. Chem. Mater. 2004; 16:581–593.
8. Aizenberg J, et al. Skeleton of Euplectella sp.: structural hierarchy from the nanoscale to the macroscale. Science. 2005; 309:275–278. doi:10.1126/science.1112255. [PubMed: 16002612]
9. Weiner S, Wagner HD. The material bone: Structure mechanical function relations. Annu. Rev. Mater. Sci. 1998; 28:271–298. doi:10.1146/annurev.matsci.28.1.271.
10. Brenner K, Arnold FH. Self-organization, layered structure, and aggregation enhance persistence of a synthetic biofilm consortium. PloS one. 2011; 6:e16791. doi:10.1371/journal.pone.0016791. [PubMed: 21347422]
11. Brenner K, Karig DK, Weiss R, Arnold FH. Engineered bidirectional communication mediates a consensus in a microbial biofilm consortium. Proceedings of the National Academy of Sciences of the United States of America. 2007; 104:17300–17304. doi:10.1073/pnas.0704256104. [PubMed: 17959781]
12. Hong SH, et al. Synthetic quorum-sensing circuit to control consortial biofilm formation and dispersal in a microfluidic device. Nature communications. 2012; 3:613. doi:10.1038/ncomms1616.
13. Ma Q, Yang Z, Pu M, Peti W, Wood TK. Engineering a novel c-di-GMP-binding protein for biofilm dispersal. Environmental microbiology. 2011; 13:631–642. doi:10.1111/j.1462-2920.2010.02368.x. [PubMed: 21059164]
14. Lee J, Jayaraman A, Wood TK. Indole is an inter-species biofilm signal mediated by SdiA. BMC microbiology. 2007; 7:42. doi:10.1186/1471-2180-7-42. [PubMed: 17511876]
15. Payne S, et al. Temporal control of self-organized pattern formation without morphogen gradients in bacteria. Molecular systems biology. 2013; 9:697. doi:10.1038/msb.2013.55. [PubMed: 24104480]
16. Payne S, You L. Engineered Cell-Cell Communication and Its Applications. Advances in biochemical engineering/biotechnology. 2013 doi:10.1007/10_2013_249.
17. Barnhart MM, Chapman MR. Curli biogenesis and function. Annu Rev Microbiol. 2006; 60:131–147. doi:10.1146/annurev.micro.60.080805.142106. [PubMed: 16704339]
18. Callura JM, Cantor CR, Collins JJ. Genetic switchboard for synthetic biology applications. Proc Natl Acad Sci U S A. 2012; 109:5850–5855. doi:10.1073/pnas.1203808109. [PubMed: 22454498]
19. Prigent-Combaret C, et al. Developmental pathway for biofilm formation in curli-producing Escherichia coli strains: role of flagella, curli and colanic acid. Environmental microbiology. 2000; 2:450–464. [PubMed: 11234933]
20. Vidal O, et al. Isolation of an Escherichia coli K-12 mutant strain able to form biofilms on inert surfaces: involvement of a new ompR allele that increases curli expression. Journal of bacteriology. 1998; 180:2442–2449. [PubMed: 9573197]
21. Hung C, et al. Escherichia coli biofilms have an organized and complex extracellular matrix structure. mBio. 2013; 4:e00645–00613. doi:10.1128/mBio.00645-13. [PubMed: 24023384]
22. Wang X, Hammer ND, Chapman MR. The molecular basis of functional bacterial amyloid polymerization and nucleation. The Journal of biological chemistry. 2008; 283:21530–21539. doi:10.1074/jbc.M800466200. [PubMed: 18508760]
23. Basu S, Gerchman Y, Collins CH, Arnold FH, Weiss R. A synthetic multicellular system for programmed pattern formation. Nature. 2005; 434:1130–1134. doi:nature03461[pii]10.1038/nature03461. [PubMed: 15858574]
24. Bacchus W LM, El-Baba MD, Weber W, Stelling J, Fussenegger M. Synthetic two-way communication between mammalian cells. Nat Biotechnol. 2012; 30:991–996. [PubMed: 22983089]
25. Tabor JJ, et al. A synthetic genetic edge detection program. Cell. 2009; 137:1272–1281. doi:S0092-8674(09)00509-1 [pii]10.1016/j.cell.2009.04.048. [PubMed: 19563759]
26. Liu C, et al. Sequential establishment of stripe patterns in an expanding cell population. Science. 2011; 334:238–241. doi:10.1126/science.1209042. [PubMed: 21998392]

NIH-PA Author Manuscript NIH-PA Author Manuscript NIH-PA Author Manuscript

27. Jang B, Park JY, Tung CH, Kim IH, Choi Y. Gold nanorod-photosensitizer complex for near-infrared fluorescence imaging and photodynamic/photothermal therapy in vivo. ACS nano. 2011; 5:1086–1094. doi:10.1021/nn102722z. [PubMed: 21244012]
28. Dreaden EC, et al. Small molecule-gold nanorod conjugates selectively target and induce macrophage cytotoxicity towards breast cancer cells. Small. 2012; 8:2819–2822. doi:10.1002/smll.201200333. [PubMed: 22777707]
29. Libutti SK, et al. Phase I and pharmacokinetic studies of CYT-6091, a novel PEGylated colloidal gold-rhTNF nanomedicine. Clinical cancer research : an official journal of the American Association for Cancer Research. 2010; 16:6139–6149. doi:10.1158/1078-0432.CCR-10-0978. [PubMed: 20876255]
30. Zakeri B, et al. Peptide tag forming a rapid covalent bond to a protein, through engineering a bacterial adhesin. Proceedings of the National Academy of Sciences of the United States of America. 2012; 109:E690–697. doi:10.1073/pnas.1115485109. [PubMed: 22366317]
31. Polman A, Atwater HA. Photonic design principles for ultrahigh-efficiency photovoltaics. Nat Mater. 2012; 11:174–177. doi:Doi 10.1038/Nmat3263. [PubMed: 22349847]
32. Reineck P, et al. A Solid-State Plasmonic Solar Cell via Metal Nanoparticle Self-Assembly. Adv Mater. 2012; 24:4750–4755. doi:DOI 10.1002/adma.201200994. [PubMed: 22740379]
33. Curto AG, et al. Unidirectional Emission of a Quantum Dot Coupled to a Nanoantenna. Science. 2010; 329:930–933. doi:DOI 10.1126/science.1191922. [PubMed: 20724630]
34. Yuan ZL, et al. Electrically driven single-photon source. Science. 2002; 295:102–105. doi:DOI 10.1126/science.1066790. [PubMed: 11743163]
35. Mao C, et al. Viral assembly of oriented quantum dot nanowires. Proceedings of the National Academy of Sciences of the United States of America. 2003; 100:6946–6951. doi:10.1073/pnas.0832310100. [PubMed: 12777631]
36. Zhang SG. Fabrication of novel biomaterials through molecular self-assembly. Nature biotechnology. 2003; 21:1171–1178. doi:10.1038/nbt874.
37. King NP, et al. Computational design of self-assembling protein nanomaterials with atomic level accuracy. Science. 2012; 336:1171–1174. doi:10.1126/science.1219364. [PubMed: 22654060]
38. Mart RJ, Osborne RD, Stevens MM, Ulijn RV. Peptide-based stimuli-responsive biomaterials. Soft Matter. 2006; 2:822–835. doi:10.1039/b607706d.
39. Webber MJ, et al. Supramolecular nanostructures that mimic VEGF as a strategy for ischemic tissue repair. Proceedings of the National Academy of Sciences of the United States of America. 2011; 108:13438–13443. doi:10.1073/pnas.1016546108. [PubMed: 21808036]
40. So CR, Tamerler C, Sarikaya M. Adsorption, diffusion, and self-assembly of an engineered gold-binding peptide on Au(111) investigated by atomic force microscopy. Angew Chem Int Ed Engl. 2009; 48:5174–5177. doi:10.1002/anie.200805259. [PubMed: 19350603]
41. Channon KJ, Devlin GL, MacPhee CE. Efficient energy transfer within self-assembling peptide fibers: a route to light-harvesting nanomaterials. Journal of the American Chemical Society. 2009; 131:12520–12521. doi:10.1021/ja902825j. [PubMed: 19678637]
42. Scheibel T, et al. Conducting nanowires built by controlled self-assembly of amyloid fibers and selective metal deposition. Proc Natl Acad Sci U S A. 2003; 100:4527–4532. doi:10.1073/pnas.0431081100 [pii]. [PubMed: 12672964]
43. Smith JF, Knowles TP, Dobson CM, Macphee CE, Welland ME. Characterization of the nanoscale properties of individual amyloid fibrils. Proc Natl Acad Sci U S A. 2006; 103:15806–15811. doi:0604035103 [pii]10.1073/pnas.0604035103. [PubMed: 17038504]
44. Felgner PL, et al. Lipofection: a highly efficient, lipid-mediated DNA-transfection procedure. Proceedings of the National Academy of Sciences of the United States of America. 1987; 84:7413–7417. [PubMed: 2823261]
45. Winfree E, Liu F, Wenzler LA, Seeman NC. Design and self-assembly of two-dimensional DNA crystals. Nature. 1998; 394:539–544. doi:10.1038/28998. [PubMed: 9707114]
46. Rothemund PW. Folding DNA to create nanoscale shapes and patterns. Nature. 2006; 440:297–302. doi:10.1038/nature04586. [PubMed: 16541064]
47. Tian B, et al. Macroporous nanowire nanoelectronic scaffolds for synthetic tissues. Nature materials. 2012; 11:986–994. doi:10.1038/nmat3404.

NIH-PA Author Manuscript

NIH-PA Author Manuscript

NIH-PA Author Manuscript

48. Hwang SW, et al. A physically transient form of silicon electronics. Science. 2012; 337:1640–1644. doi:10.1126/science.1226325. [PubMed: 23019646]

49. Amsden JJ, et al. Rapid nanoimprinting of silk fibroin films for biophotonic applications. Adv Mater. 2010; 22:1746–1749. doi:10.1002/adma.200903166. [PubMed: 20496408]

50. Lutolf MP, Hubbell JA. Synthetic biomaterials as instructive extracellular microenvironments for morphogenesis in tissue engineering. Nature biotechnology. 2005; 23:47–55. doi:10.1038/nbt1055.

51. Prewitz MC, et al. Tightly anchored tissue-mimetic matrices as instructive stem cell microenvironments. Nature methods. 2013; 10:788–794. doi:10.1038/nmeth.2523. [PubMed: 23793238]

52. Chiu WK, Yu KM. Direct digital manufacturing of three-dimensional functionally graded material objects. Computer-Aided Design. 2008; 40:1080–1093.

53. Xia Y, Rogers JA, Paul KE, Whitesides GM. Unconventional Methods for Fabricating and Patterning Nanostructures. Chemical reviews. 1999; 99:1823–1848. [PubMed: 11849012]

54. Kolodkin-Gal I, et al. D-amino acids trigger biofilm disassembly. Science. 2010; 328:627–629. doi:10.1126/science.1188628. [PubMed: 20431016]

55. Gubeli RJ, Burger K, Weber W. Synthetic biology for mammalian cell technology and materials sciences. Biotechnology advances. 2013; 31:68–78. doi:10.1016/j.biotechadv.2012.01.007. [PubMed: 22286074]

NIH-PA Author Manuscript

NIH-PA Author Manuscript

NIH-PA Author Manuscript

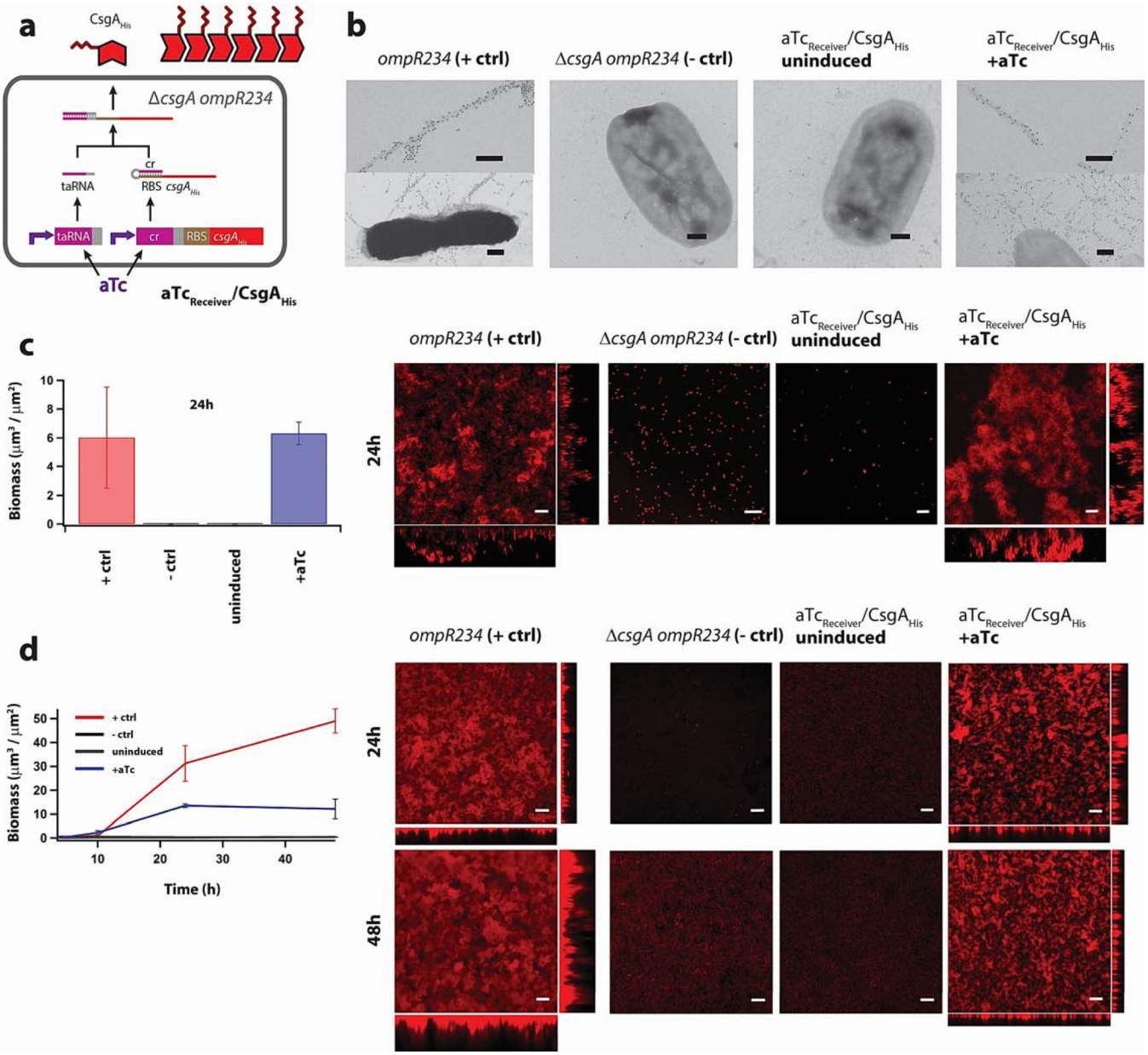

Figure 1. Inducible production of engineered curli fibrils and biofilms

a, Riboregulator circuits tightly regulate expression of curli subunits, such as $CsgA_{His}$. Production of $CsgA_{His}$ requires the expression of *trans*-activating RNA (taRNA). The taRNA prevents the *cis*-repressive (cr) sequence from blocking the ribosome-binding sequence (RBS) controlling translation of the mRNA transcript. In the absence of inducer, mRNA and taRNA levels are low, thus leading to significant repression of gene expression. The addition of aTc induces transcription of both $csgA_{His}$ mRNA and taRNA, thus enabling $CsgA_{His}$ production. Tight regulation of curli expression is useful for controlling patterning (Supplementary Fig. 19). **b,** Immuno-labelling of curli fibrils with rabbit anti-CsgA antibodies and gold-conjugated goat anti-rabbit antibodies. Positive-control ("+ ctrl") MG1655 *ompR234* cells ("*ompR234*", see Supplementary Table 3), which have an intact

NIH-PA Author Manuscript

NIH-PA Author Manuscript

NIH-PA Author Manuscript

endogenous *csgA* gene, produce curli fibrils that were labelled by anti-CsgA antibodies and are attached to cells. However, negative-control ("− ctrl") cells with the *csgA* gene knocked out and no *csgA*-expressing circuits ("Δ*csgA ompR234*", see Supplementary Table 3), as well as $aTc_{Receiver}/CsgA_{His}$ cells in the absence of aTc, did not produce curli fibrils. Inducing $aTc_{Receiver}/CsgA_{His}$ cells with aTc enabled the synthesis of curli fibrils that were labelled by anti-CsgA antibodies and attached to cells. Scale bars are 200nm. **c,** Confocal microscopy and biomass quantification revealed that under static culture conditions, *E. coli ompR234* cells formed thick adherent biofilms. However, *E. coli* Δ*csgA ompR234* cells, as well as $aTc_{Receiver}/CsgA_{His}$ cells in the absence of aTc, did not form biofilms. Inducing $aTc_{Receiver}/CsgA_{His}$ cells with aTc led to the formation of thick adherent biofilms. **d,** Confocal microscopy and biomass quantification revealed similar biofilm-forming capabilities by *E. coli ompR234* and induced $aTc_{Receiver}/CsgA_{His}$ cells when grown in flow cells. To enable visualization, we transformed a constitutive mCherry-expressing plasmid into all strains (see Supplementary Methods). Cells were grown in liquid M63 media with glucose; the corresponding experiments for other media conditions are shown in Supplementary Figure 1 and 2. Scale bars in c) and d) are 50μm, and orthogonal XZ and YZ views are maximum-intensity projections.

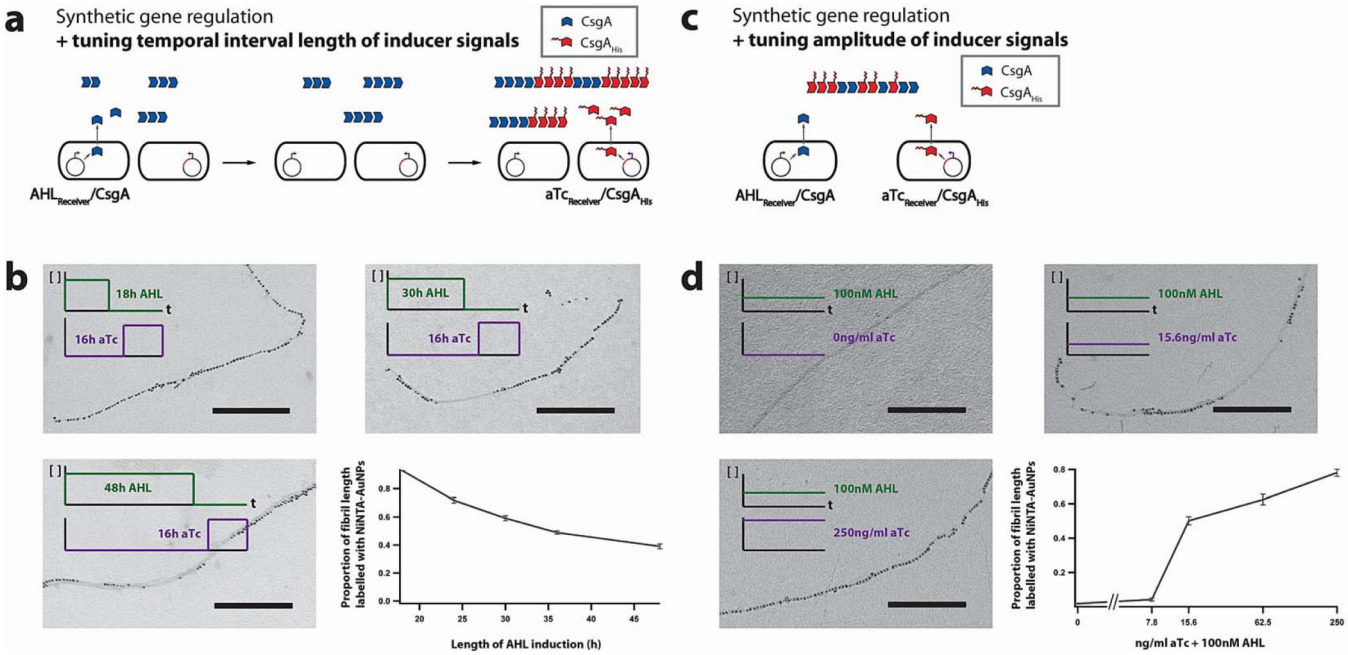

Figure 2. Conversion of timing and amplitude of chemical inducer signals into material structure and composition

a, Inducible synthetic gene circuits couple curli subunit secretion to external chemical inducers. Engineered cells containing these circuits can translate induction pulse length into nanoscale structure and composition of block co-fibrils. **b,** We first used AHL to induce secretion of CsgA from $AHL_{Receiver}$/CsgA and then used aTc to induce secretion of $CsgA_{His}$ from $aTc_{Receiver}$/$CsgA_{His}$. We tuned the relative block lengths and proportions of CsgA and $CsgA_{His}$ (plot of the proportion of fibril length labelled by NiNTA-AuNP, solid grey line) by changing the relative lengths of AHL versus aTc induction times. Scale bars are 200nm. **c,** Synthetic genetic regulatory circuits that couple curli subunit secretion to external inducer signals can translate inducer concentration into nanoscale structure and composition of block cofibrils. **d,** Engineered cells AHL induced secretion of CsgA from $AHL_{Receiver}$/CsgA, while at the same time, aTc induced secretion of $CsgA_{His}$ from $aTc_{Receiver}$/$CsgA_{His}$. We tuned the relative block lengths and proportions of CsgA and $CsgA_{His}$ by changing the relative concentrations of AHL and aTc inducers applied simultaneously. The solid grey line indicates the proportion of fibril length labelled by NiNTA-AuNP with varying concentrations of aTc and constant 100nM AHL. Detailed histograms can be found in Supplementary Figure 6. Scale bars are 200nm.

NIH-PA Author Manuscript NIH-PA Author Manuscript NIH-PA Author Manuscript

NIH-PA Author Manuscript

NIH-PA Author Manuscript

NIH-PA Author Manuscript

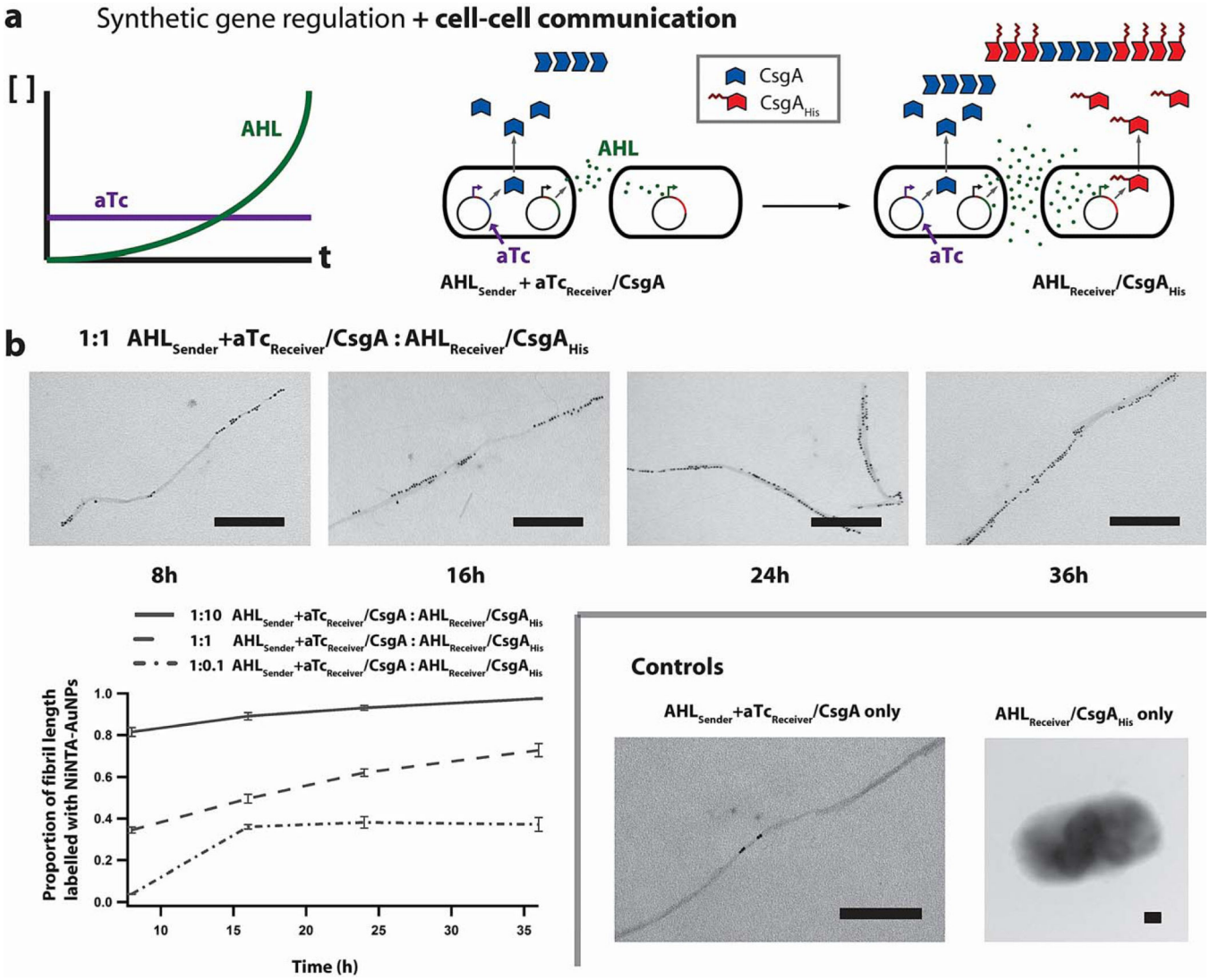

Figure 3. Synthetic cellular communication for dynamic, autonomous material production and patterning

a, Synthetic gene circuits that couple curli subunit secretion to external inducer signals, when combined with synthetic cellular communication circuits, allow for the production of materials whose structure and composition changes autonomously with time. AHL_{Sender}+$aTc_{Receiver}$/CsgA secreted both CsgA and AHL. As AHL signal accumulated, $AHL_{Receiver}$/$CsgA_{His}$ secreted increasing levels of $CsgA_{His}$. **b,** Using the autonomous cellular communication system, the length of $CsgA_{His}$ blocks and the proportion of $CsgA_{His}$ increased with time (plot of the proportion of fibril length labelled by NiNTA-AuNP, grey lines). This behaviour could be tuned by the ratio of the seeding density of AHL_{Sender}+$aTc_{Receiver}$/CsgA cells to $AHL_{Receiver}$/$CsgA_{His}$ cells. When only AHL_{Sender}+$aTc_{Receiver}$/CsgA cells were present, the resulting fibrils were almost uniformly unlabelled; when only $AHL_{Receiver}$/$CsgA_{His}$ cells were present, no curli fibrils were formed (Controls). Detailed histograms can be found in Supplementary Fig. 10. Scale bars are 200nm.

NIH-PA Author Manuscript

NIH-PA Author Manuscript

NIH-PA Author Manuscript

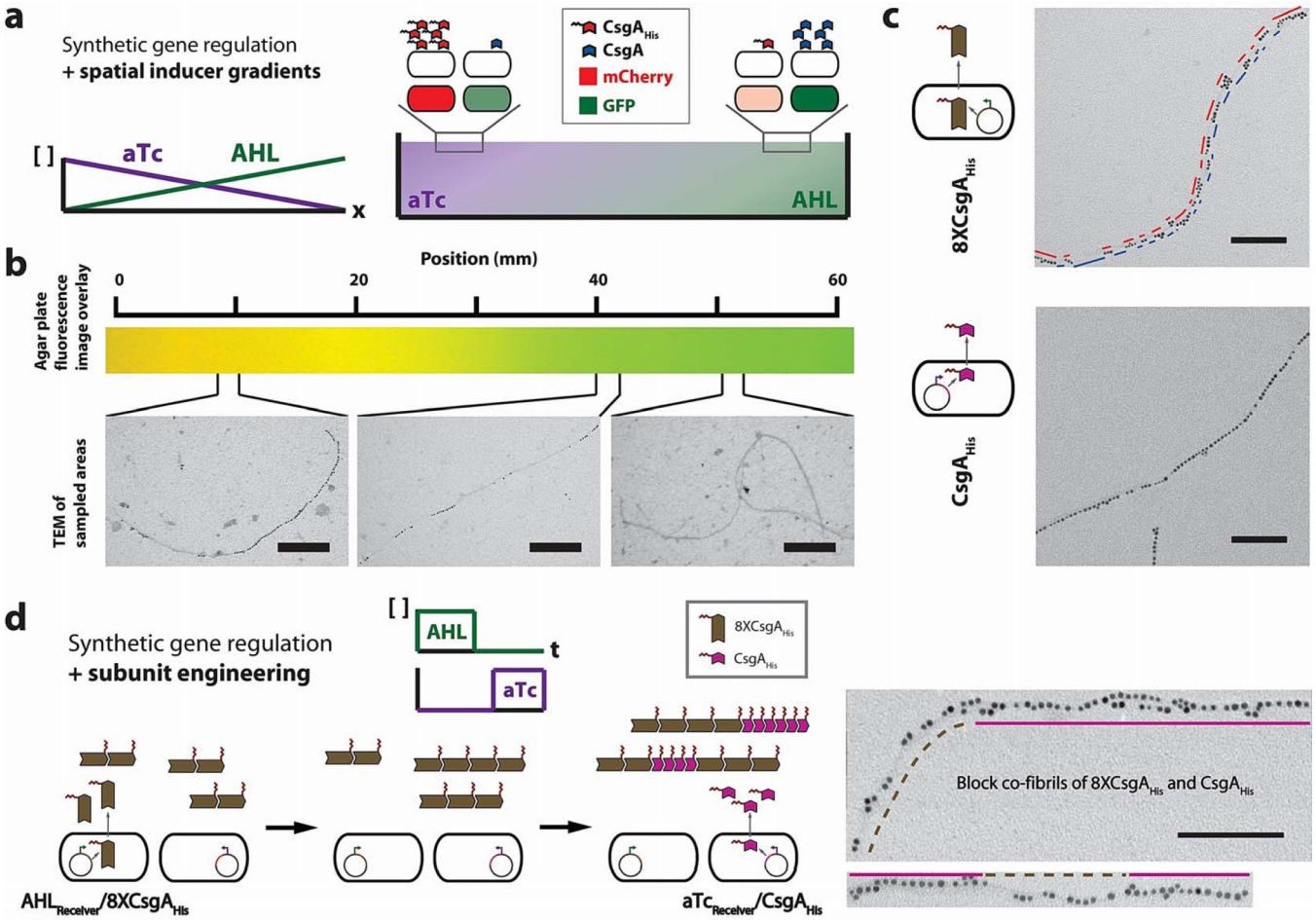

Figure 4. Multiscale patterning with cellular consortia via synthetic gene regulation combined with inducer gradients and subunit engineering

a, Synthetic gene circuits that couple curli subunit secretion to external inducer signals, when combined with a spatial inducer gradient, enable patterning across multiple length scales. We used an agar plate with opposing concentration gradients of AHL and aTc to achieve control at the macroscale (Supplementary Fig. 12). This was combined with regulation of nanoscale patterning to achieve multiscale patterning. Embedded in top agar were equal numbers of $AHL_{Receiver}$/CsgA, $aTc_{Receiver}$/$CsgA_{His}$, $AHL_{Receiver}$/GFP, and $aTc_{Receiver}$/mCherry cells. **b,** By combining synthetic gene regulation with spatial inducer gradients, we created a change in the nanoscale structure of fibrils across a distance of millimetres. This nanoscale and macroscale patterning was shown by changes in segment lengths of unlabelled and NiNTA-AuNP-labelled fibril segments at different locations across the agar plate. Inducer concentration gradients were demonstrated by overlaid GFP and mCherry fluorescence images of embedded $AHL_{Receiver}$/GFP and and $aTc_{Receiver}$/mCherry reporter cells. Scale bars are 200nm. **c,** We also achieved patterning at the nanoscale by protein engineering of curli subunits. Concatenating eight tandem repeats of CsgA and adding one histidine tag to the C-terminus ($8XCsgA_{His}$) resulted in fibrils that were labelled by a syncopated pattern of NiNTA-AuNPs, with clusters of particles separated by 33.3±27.1 (s.e.m.) nm. Scale bars are 100nm. **d,** Synthetic gene circuits that couple curli

NIH-PA Author Manuscript

NIH-PA Author Manuscript

NIH-PA Author Manuscript

subunit secretion to external inducer signals, when combined with subunit engineering, enable patterning across multiple length scales (nanometres to micrometres). We used AHL to induce production of $8XCsgA_{His}$ from $AHL_{Receiver}/8XCsgA_{His}$ and then used aTc to induce production of $CsgA_{His}$ from $aTc_{Receiver}/CsgA_{His}$. In the TEM images, dashed brown lines refer to syncopated $8XCsgA_{His}$ segments while the solid amethyst lines indicate $CsgA_{His}$ segments. Detailed histograms for data shown here can be found in Supplementary Figure 11. Scale bars are 100nm.

NIH-PA Author Manuscript

NIH-PA Author Manuscript

NIH-PA Author Manuscript

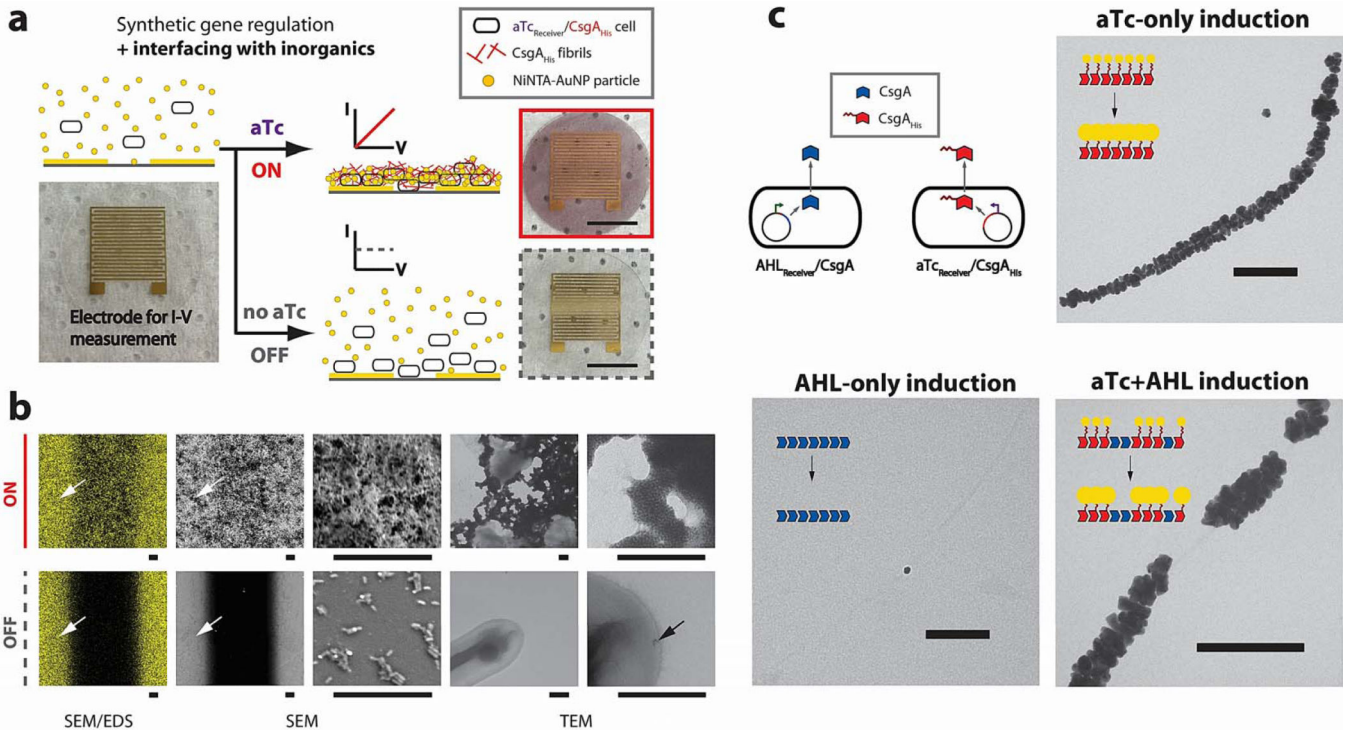

Figure 5. Environmentally switchable conductive biofilms and cell-based synthesis of curli-templated nanowires and nanorods

a, We used $aTc_{Receiver}/CsgA_{His}$ cells to form amyloid fibrils composed of $CsgA_{His}$ in response to aTc. When combined with NiNTA-AuNPs, we created conductive biofilms that can be externally controlled as electrical switches. When aTc was added to $aTc_{Receiver}/CsgA_{His}$ cells grown in the presence of NiNTA-AuNPs, it triggered the formation of conductive biofilms on electrodes, with embedded 5nm gold particles giving biofilms a red colour (‘ON’, solid red box). However, in the absence of aTc, few cells adhered to the electrodes (‘OFF’, dashed grey box). Scale bars are 5mm. **b,** SEM/EDS elemental mapping of the aTc-induced ‘ON’ state for $aTc_{Receiver}/CsgA_{His}$ biofilms showed that networks of gold in the biofilms connected the electrodes (white arrows). SEM imaging showed that the biofilms bridged electrodes. TEM imaging showed networks of aggregated gold particles. In contrast, SEM/EDS mapping of the ‘OFF’ state showed no gold networks, SEM imaging showed only scattered cells in the gap between electrodes, and TEM imaging showed only scattered and isolated gold particles (black arrow). Scale bars of scanning electron micrographs are 20μm and scale bars of transmission electron micrographs are 200nm. **c,** A mixed population of $aTc_{Receiver}/CsgA_{His}$ and $AHL_{Receiver}/CsgA$ cells produced curli templates for organizing either gold nanowires or gold nanorods when they were induced with aTc only or both aTc and AHL, respectively. NiNTA-AuNPs were patterned on $CsgA_{His}$ subunits within curli fibrils and then gold enhanced. Scale bars are 200nm.

NIH-PA Author Manuscript

NIH-PA Author Manuscript

NIH-PA Author Manuscript

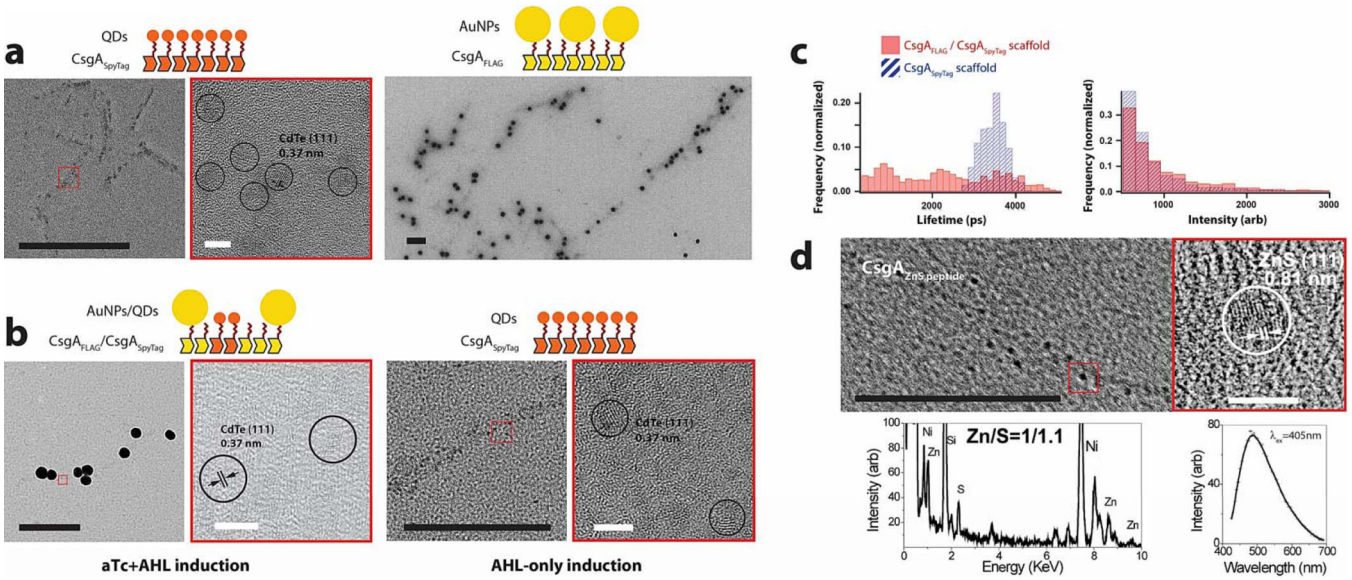

Figure 6. Assembly and tuning of functional AuNP-QD heterostructures and nucleation of fluorescent ZnS QDs on cell-synthesized curli fibrils

a, $CsgA_{SpyTag}$ fibrils specifically bind CdTe/CdS QDs conjugated to the SpyCatcher protein; the CdTe cores of QDs are seen under HRTEM. $CsgA_{FLAG}$ fibrils are specifically bound by anti-FLAG antibodies which are in turn bound by 40nm AuNPs conjugated to secondary antibodies. CsgA fibrils do not bind either CdTe/CdS QDs conjugated to SpyCatcher or 40nm AuNPs conjugated to antibodies (Supplementary Fig. 23a, b). **b,** A mixed population of $aTc_{Receiver}/CsgA_{FLAG}$ and $AHL_{Receiver}/CsgA_{SpyTag}$ cells produced curli templates for either AuNP-QD heterostructures (cofibrils of $CsgA_{FLAG}$ and $CsgA_{SpyTag}$) or QD-only assemblies ($CsgA_{SpyTag}$ fibrils) depending on whether they were induced by both aTc and AHL, or AHL only, respectively. **c,** Cell-patterned curli fibrils enable the tuning of stimuli-responsive inorganic-organic materials. AuNP-QD assemblies patterned on $CsgA_{FLAG}/CsgA_{SpyTag}$ scaffolds (solid red bars) exhibited different fluorescence lifetime and intensity properties than QD-only assemblies patterned on $CsgA_{SpyTag}$ scaffolds (hashed blue bars). **d,** $CsgA_{ZnS\ peptide}$ fibrils nucleated ~5nm nanoparticles with a cubic zinc blende ZnS (111) structure and approximately 1:1 ratio of zinc and sulphur. The particles were fluorescent, with an emission peak at 490nm when excited at 405nm. Control CsgA fibrils nucleated few such particles (Supplementary Fig. 23c). In a), b), and d) black scale bars are 200nm and white scale bars are 5nm; the images outlined by red boxes are zoomed-in versions of the inset red boxes.